IOP Publishing Nanotechnology

Nanotechnology **27** (2016) 125303 (8pp) doi:10.1088/0957-4484/27/12/125303

Ordered $La_{0.7}Sr_{0.3}MnO_3$ nanohole arrays fabricated on a nanoporous alumina template by pulsed laser ablation

M Kumaresavanji[1], I T Gomes[1], A Apolinario[1], A G Rolo[2], B G Almeida[2], A M L Lopes[1] and J P Araujo[1]

[1] IFIMUP and IN-Institute of Nanoscience and Nanotechnology, Department of Physics and Astronomy, Faculty of Sciences, University of Porto, Porto, Portugal
[2] Centro de Fisica, Universidade do Minho, Campus de Gualtar, 4710–057 Braga, Portugal

E-mail: vanji.hplt@gmail.com

Received 24 July 2015, revised 13 January 2016
Accepted for publication 14 January 2016
Published 18 February 2016

Abstract

Highly ordered nanohole arrays of $La_{0.7}Sr_{0.3}MnO_3$ manganite have been synthesized using pulsed laser deposition on nanoporous alumina template. Their structure and phase formation were characterized by scanning electron microscopy (SEM), atomic force microscopy (AFM), energy dispersive x-ray spectroscopy (EDX) and x-ray diffraction (XRD). The magnetic measurements were performed with respect to temperature and field and exhibit a ferromagnetic to paramagnetic transition at 284 K. In addition, the temperature dependence of electrical resistance was measured at different magnetic fields and an insulating phase throughout all the temperatures was observed. The low temperature ferromagnetic insulating state is discussed by the presence of a canted ferromagnetic state induced by the nanoholes. The present work shows the feasibility of combining both the nanoporous alumina template and pulsed laser ablation for the fabrication of perovskite manganite nanohole arrays which can also be extended to fabricate other multicomponent oxide nanohole materials.

Keywords: perovskite manganite, anodic aluminium oxide, nanostructures, magnetic properties

(Some figures may appear in colour only in the online journal)

1. Introduction

Nanostructured materials that offer huge surface to volume ratio have proved to be potential candidates in the development of modern technology and can be found in many applications such as drug delivery, hyperthermia, fuel cells, supercapacitors, hydrogen storage systems and magnetic refrigeration [1–4]. In this context, the synthesis and design of nanoscale structures have attracted much attention due not only to their potential applications but also for their size dependent physical properties. Continuous films with nano-sized voids, called nanohole arrays, are one example of such interesting nanostructured materials which exhibit enhanced exchange bias, modified magnetization reversal, increased coercivity and the unusual domain wall pinning effect [5–7]. Such nanoholes generate magnetic charges in their vicinity and create stray field that promotes local magnetization reversal by magnetization rotation. The nanohole arrays are also potentially important in the sense of enhancing the data density of magnetic storage media because of their shape anisotropy along with the intrinsic uniaxial anisotropy [8, 9]. Furthermore, in these structures the superparamagnetic limit is nonexistent [6].

Such nanohole arrays have been prepared by a wide variety of methods: self-assembly of sputter-deposited films, focused ion beam deposition, electron-beam lithography and nano-imprinting [10–13]. In most cases, the pre-patterned nanoporous alumina (NPA) was widely used as template to produce such nanohole arrays due to the ability to control the size of the pores and the fact that the production of the templates is an easy and versatile process [14]. So far, a number of investigations were carried out on nanohole arrays

of single ferromagnets (e.g. permalloys, CoCrPt) and multilayered porous materials [5–13]. However, such studies in multicomponent oxide materials are scarce due to the general difficulty in processing the oxides using the above mentioned methods.

Here, we report the fabrication of perovskite $La_{0.7}Sr_{0.3}MnO_3$ (LSMO) nanohole arrays by pulsed laser deposition on an NPA template and investigated their structural, magnetic and charge transport properties. For the purposes of comparison, a continuous thin film of LSMO on a MgO substrate was also prepared and its charge transport and magnetic properties were compared with the nanohole arrays. Perovskite manganites are well known for their very large magnetoresistance that have made them suitable for spintronic devices [15, 16]. In particular, Sr doped $La_{1-x}Sr_xMnO_3$ with $x = 0.3$ is a ferromagnetic metal at room temperature and possesses a very high degree of spin polarization. Therefore, it is considered a candidate for diverse potential applications, such as electrodes for solid oxide fuel cells, hyperthermia, magnetic refrigeration or magnetic recording media [17–19]. Hence, it is quite interesting to investigate the effect of surface modification on LSMO thin films in order to develop such nanostructured materials for potential applications.

2. Experimental details

The NPA template was prepared by a standard two step anodization process using phosphoric acid as an electrolyte as described elsewhere [20]. In this method, NPA templates with a thickness of 30 μm and nanopore diameter of 190 nm were grown. The inter-pore distance was 500 nm. The polycrystalline target of LSMO for thin film deposition was prepared by a solid state reaction method. Stoichiometric amounts of MnO_2, La_2O_3 and $SrCO_3$ were suspended in ethanol and mixed in a planetary Retsch PM400 ball mill for 5 hours at a speed of 180 rpm. The homogenized suspension was dried for 12 h at a temperature of 90 °C. The obtained powder was successively pelletized and annealed several times at increasing temperatures up to 1500 °C in order to eliminate the carbonates and obtain a dense pellet.

The film deposition on NPA was performed by pulsed laser ablation, using a KrF excimer laser with $\lambda = 248$ nm and a pulse duration of 25 ns, at a laser fluence of 2 Jcm^{-2} on the target. The laser repetition rate was 3 Hz and the target-to-substrate distance was 5 cm. Prior to deposition, the substrates were cleaned in an ultra-sound bath with ethanol. They were then put in the ablation chamber which was evacuated to a base pressure of 10^{-5} mbar. During the deposition the substrate temperature was 700 °C and the oxygen pressure was 0.8 mbar. To better clean the substrates, they were kept at 700 °C for 30 min before deposition, for degasification. These preparation conditions allow the preparation of dense, homogeneous LSMO thin films, with low droplet density in a controlled way [21, 22]. To prevent under-oxidation of the films after deposition they were cooled down to room temperature, at a rate of 7 °Cmin^{-1}, under an atmospheric oxygen pressure. The final sample size was 0.79 cm^2 .

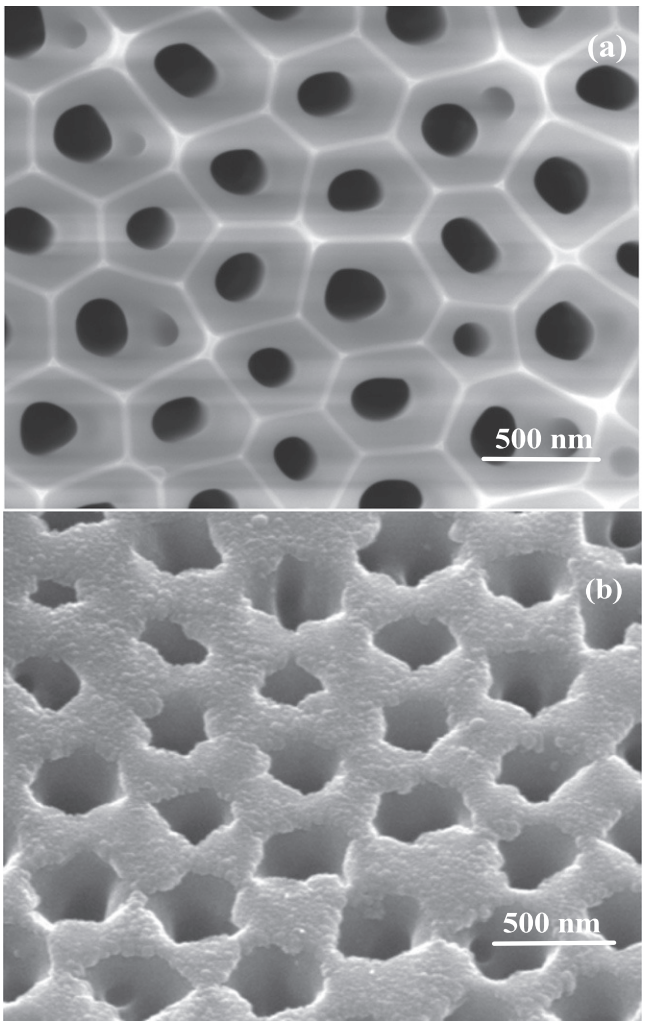

Figure 1. SEM micrographs of a prepared NPA template (a) and LSMO nanohole arrays (b).

The morphology of as prepared nanohole arrays was examined by scanning electron microscopy (SEM) using FEI Quanta 400FEG. The topographic profiles and surface roughness (R_q) were analyzed using a nanoscope multimode atomic force microscope from Veeco Instruments. The AFM profiles were analysed using the nanoscope multimode atomic force microscope software to determine the thickness of nanohole arrays. The phase purity was verified using EDX and XRD. Magnetic behaviors with respect to temperature and field were studied using a commercial SQUID magnetometer. The electrical resistance with respect to temperature at different magnetic field was measured by two probe method using a closed cycle refrigerator. The electrical contacts were made by Cu wire and silver epoxy. The magnetic field was parallel to the electrical current applied in the plane of the sample.

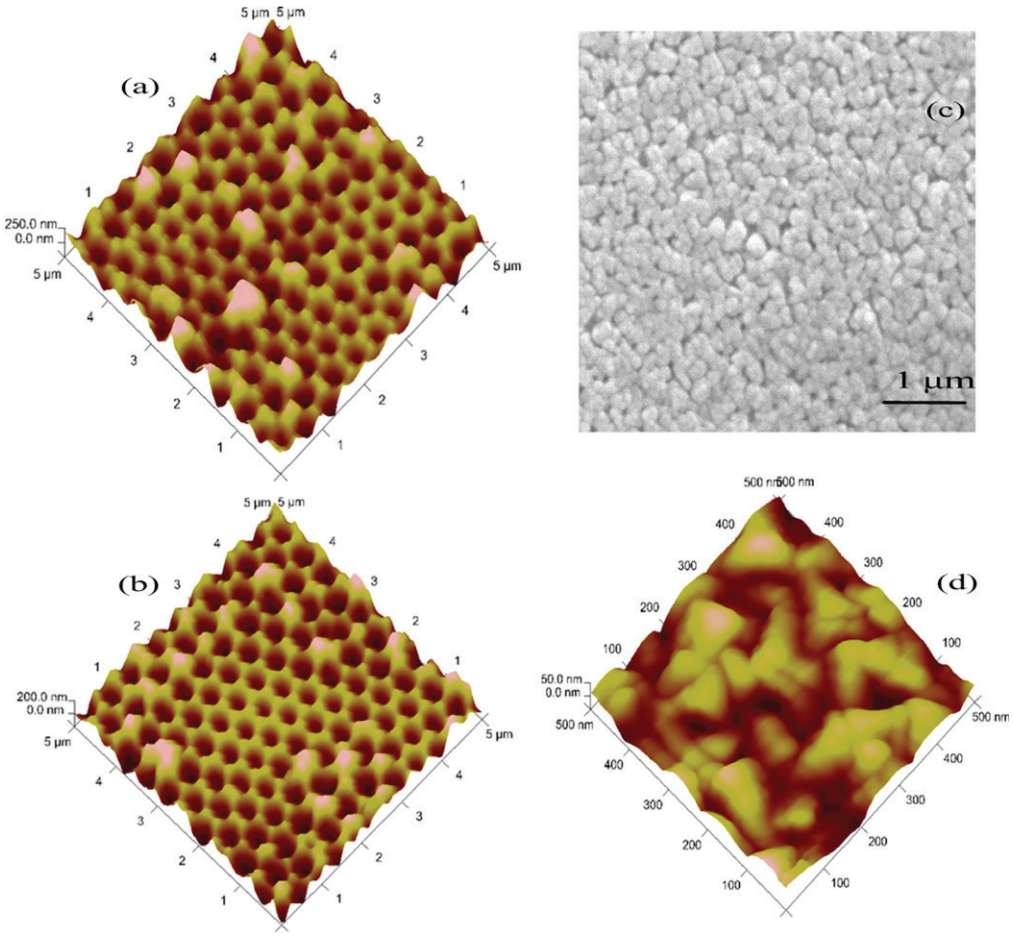

Figure 2. Surface topography of (a) NPA template (b) LSMO nanohole arrays, (c) top view SEM micrograph of LSMO/MgO film and (d) continuous LSMO/MgO film obtained using AFM.

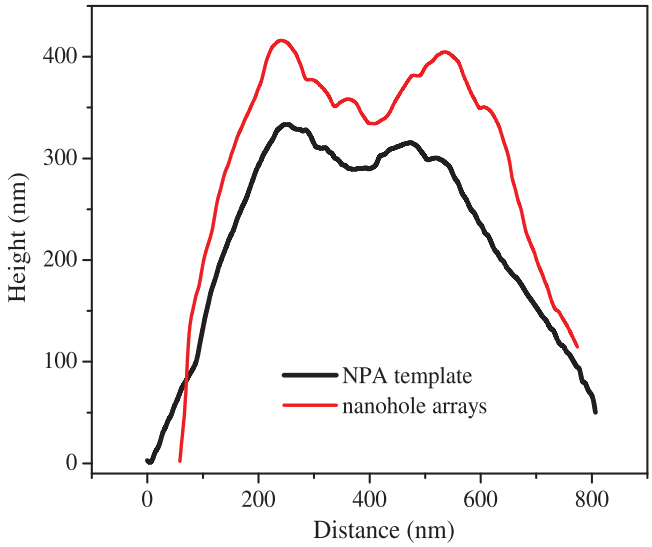

Figure 3. Representative profile height of NPA template and LSMO nanohole arrays extracted from figures 2(a) and (b).

3. Results and discussion

Figure 1(a) shows the top view SEM micrograph of NPA template prior to thin film deposition. From the figure, it can be seen well defined regular nanopore arrays with a pore diameter of about 190 ± 10 nm and an interpore distance of 500 nm. Figure 1(b) shows the surface SEM micrograph of as prepared LSMO nanohole arrays deposited on NPA. As seen from figure 1(b), the film is continuous and uniform for this thickness. The average diameter of the nanoholes is 160 nm which is less than the average nanopore diameter due to the deposition of the film around the pores' perimeters. The cross section SEM micrographs, which are not shown here, display that very little LSMO enters the template pores and it is essentially concentrated at the surface, replicating the template. In figures 2(a) and (b), we present the AFM topography images of the NPA template and LSMO nanohole arrays, respectively. The nanohole arrays replicate the NPA template and the film was grown on the surface between the nanopores of NPA. As seen from the figure, the six hills on the nanopores perimeter are also replicated by the deposited film. Some bright beads can also be seen in the AFM images that are defects points on the sample, characteristic of NPA templates. The AAO shows hexagonal domains that are interrupted by defects associated with grain boundaries of the Al and thereby the thin film deposited also exhibit the same defects.

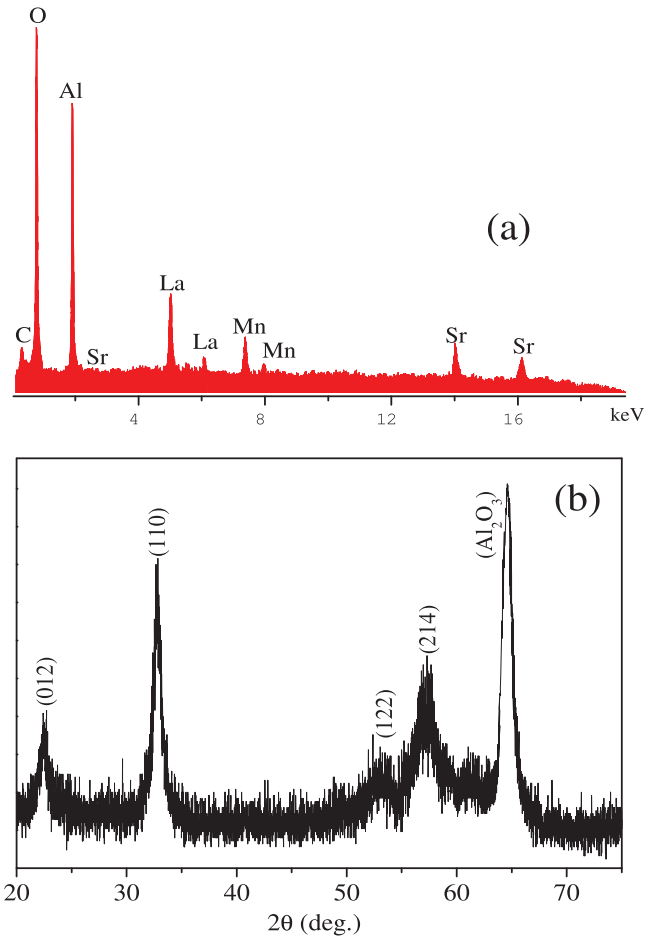

Figure 4. EDX analysis (a) and XRD pattern (b) for LSMO nanohole arrays.

The mean film thickness was obtained by the AFM image section profile analyses by subtracting the profile mean height of the LSMO nanohole arrays from NPA template profile mean height. Figure 3 shows such representative AFM images profiles of both samples. The AFM height profile was obtained by averaging in five different areas of the AFM images (figure 2 with (a) and without (b) film) and the mean thin film thickness obtained was of 89 nm. The average surface roughness R_q was extracted from the AFM topography of the image 5×5 μm areas and is defined as the root-mean-square value of the image pixel height which results in a significant R_q of 95 nm for the NPA template (figure 2(a)). After the thin film deposition, a smoother surface was obtained, with an R_q of 82 nm (figure 2(b)), which is in good agreement with those observed by SEM. Thus, it can be observed that the hexagonal hill-like surface that characterize nanoporous alumina templates becomes smoother after thin film deposition.

Figure 4(a) shows the EDX spectra obtained from LSMO nanohole arrays. The peaks in the spectra can be indexed to La, Sr, Mn and O which correspond to the LSMO nanohole arrays. In the spectrum, C and Al peaks can also be seen which are from carbon glue used to fix the sample and the NPA template, respectively. The obtained La:Sr:Mn ratio was 0.68:0.32:1 which is in good agreement with the $La_{0.7}Sr_{0.3}MnO_3$ nominal composition. The XRD pattern of as prepared LSMO nanohole arrays that was recorded at room temperature is depicted in figure 4(b). The reflection peaks could be indexed with two kinds of peak associated to a rhombohedral perovskite structure of LSMO with space group R3c and $\gamma - Al_2O_3$. Such indexed peaks are consistent with the reported ones [23]. The absence of any other peaks confirms the phase purity of the as prepared LSMO nanohole arrays.

For comparison purposes, we have also prepared a continuous LSMO thin film on a MgO substrate, under the same conditions and deposition time as the one prepared over the NPA template. The top view SEM micrograph and AFM topography of the LSMO/MgO thin film are presented in figures 2(c) and (d), respectively. The thickness of LSMO/MgO thin film was determined from the cross-sectional SEM micrograph and the obtained thickness is about 130 nm. The same is also confirmed from the low angle x-ray reflectometry. The surface roughness was estimated from the AFM topography (figure 2(d)) which was estimated as 15 nm. The R_q in the continuous film is much lower than in the nanohole arrays and evidences a better surface smoothness. Since the nanohole arrays reproduce the underlying hexagonal pattern of NPA template and replicate the hills that surround the nanopores, the R_q is much higher compared to the continuous film deposited on MgO substrate. Additionally, the higher roughness on the nanohole arrays can also explain the difference in average thickness as compared to the continuous film.

In figure 5, we show the magnetization measurements of the LSMO nanohole arrays with field applied in-plane (IP) and out-of-plane (OP) of the arrays. Figure 5(a) exhibits a temperature dependence of magnetization ($M(T)$) curves of field cooled (FC) and zero field cooled (ZFC) with the field of 500 Oe. From the obtained curves, a ferromagnetic to paramagnetic transition (T_C) at 284 K was observed and such a T_C value is lower than that of a continuous LSMO/MgO thin film (293 K) as displayed in figure 5(c). The magnetic behavior is different for fields applied in-plane and out-of-plane to both of the samples and confirms the anisotropic magnetic behavior of LSMO nanohole arrays and the LSMO/MgO film.

In addition, we have measured the field dependence of magnetization ($M(H)$) with the field applied along the in-plane and out-of-plane of the LSMO nanohole arrays and LSMO/MgO film at 5 K and the results are shown in figures 5(b) and (d), respectively. The measurements show that the samples are ferromagnetic at 5 K and confirm in-plane anisotropy. In addition, large coercive fields (H_C) of 48 mT and 127 mT were observed for fields out-of-plane and in-plane to the nanohole arrays, respectively, which is much higher than the observed H_C in continuous LSMO/MgO films, which are 29 and 41 mT for field applied out-of-plane and in-plane, respectively. From the measurements, it is evident that the easy magnetization axis of both samples lies within the sample plane.

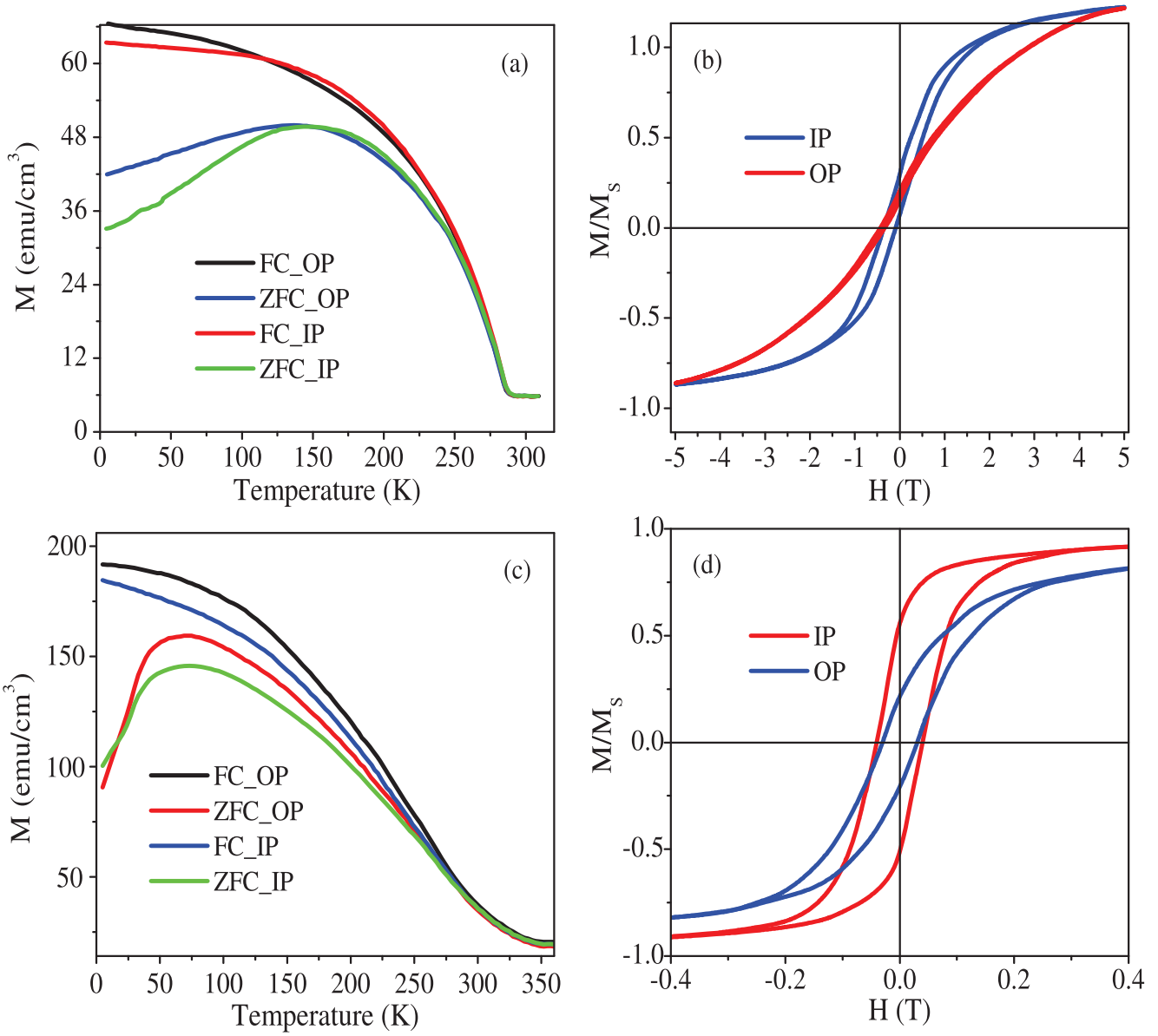

Figure 5. Temperature dependence of magnetization for (a) LSMO nanohole arrays and (c) LSMO/MgO continuous film. Field dependence of magnetization for (b) LSMO nanohole arrays and (d) LSMO/MgO film.

In order to study the charge transport mechanism in nanohole arrays, we have measured the temperature dependence of electrical resistance ($R(T)$) at different external fields and the obtained results are shown in figure 6(a). The resistance increases abruptly by decreasing the temperature and at below 150 K it tends to stabilize. As seen from the curves, the sample shows an insulating-like behavior throughout the whole temperature range. This is related to an enhanced grain boundary contribution in the nanohole arrays [24], as confirmed by the higher magnetoresistance at lower temperatures when compared to the magnetoresistance in the vicinity of T_C. In fact, the change in resistance value near the magnetic transition is smaller even for the field of 0.8 T, as shown in figure 6(a). However, the field suppresses the resistance monotonically at a rate of $dR/dH = 21\ \Omega/\text{Oe}$ at lower temperatures. This higher reduction of resistance at lower temperatures $T < T_C$ confirms that the grain boundary magnetoresistance dominates over intrinsic colossal magnetoresistance [25].

In contrast, the continuous LSMO/MgO film exhibits a metal–insulator transition (T_{MI}) at 231 K as determined from the $R(T)$ measurements shown in figure 6(b). The T_{MI} is much lower than the Curie temperature (figure 5(c)) and hinders the gradual increase of ferromagnetism and hence the ferromagnetic metallic state is only attained at T_{MI}. The upturn observed at lower temperatures ($T < 80$ K) is associated with the dominance of the grain bounday contribution. The resistance of such a grain boundary is considerably higher in the low temperature region that scatters the charge carriers and reduces the conductivity [26].

Indeed, the nanosized grains provide a larger surface for a specific volume and should enable better intercalation of

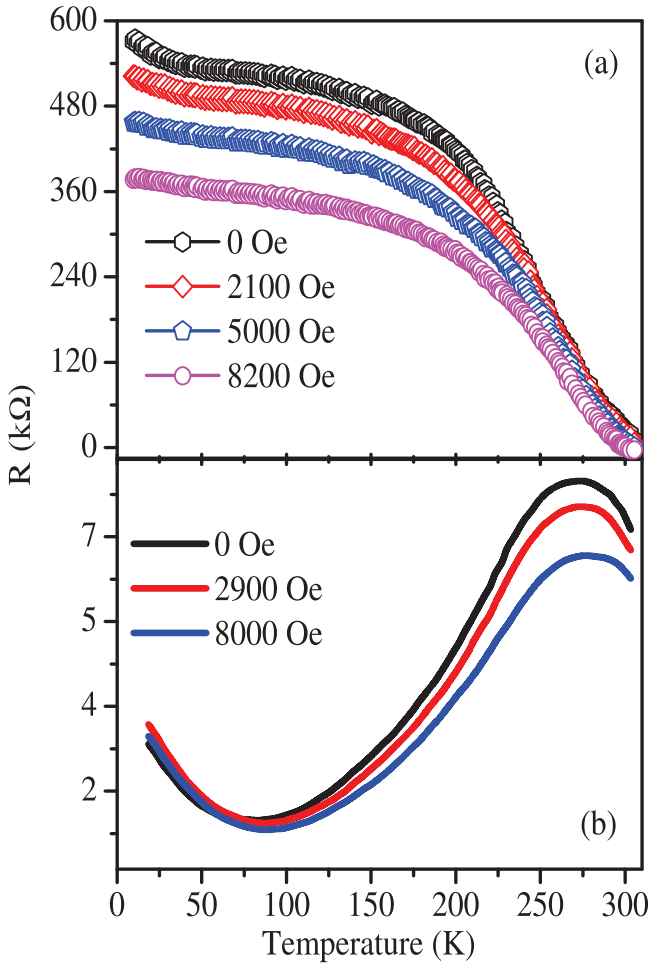

Figure 6. Temperature dependence of resistance for (a) LSMO nanohole arrays and (b) LSMO/MgO film at different fields.

charges in nanostructured materials. However, a large number of grain boundaries occurred in these materials which act as insulating barrier layers. Previous studies reported that the electrical conduction in granular films takes place by electron tunneling across the grain boundaries [27]. Such tunneling is strongly dependent on the alignment of the magnetic moments of two consecutive grains and extremely sensitive to an applied magnetic field. According to the Jullieres model [28], the electron transport is higher when the grains are ferromagnetically coupled and lower for the anti-parallel orientation. Here, we observed a ferromagnetic insulating behavior for nanohole arrays and a ferromagnetic metallic state for continuous LSMO/MgO film. This unusual insulating behavior of nanohole arrays can be explained by the canted ferromagnetic state which is induced by the nanoholes and restricts the transport behavior. The observed higher resistance values also provide evidence for the enhanced grain boundary contribution as mentioned earlier. The resistance is reduced upon application of an external magnetic field because of the increased alignment of the spins that gives rise to increased inter-grain transport.

It is well known that the physical properties of nanostructured materials are different when compared with the bulk one due to their higher surface to volume ratio. In particular, nanohole arrays exhibit peculiar physical properties because of the presence of voids in thin film which can be seen from the obtained results in the present work. According to previous reports, two different magnetic regions can occur in the nanohole arrays due to the presence of voids [7–9, 29]. One is the magnetically ordered state between the holes and another one is the spin misalignment region in the vicinity of the holes. Such magnetic phase separation reduces T_C when compared to the continuous LSMO/MgO thin films. This reduction in T_C is also much lower compared to other LSMO continuous thin films reported with different substrates [21, 24, 26]. Such reduction in the T_C value can also be explained by the voids which create a magnetic pinning effect and thereby reduce the domain size as reported earlier [5, 9, 29]. These voids act as volume defects and limit the magnetic domain size by confining the domain walls. That magnetic pinning effect obtained by nanoholes not only decreases the T_C but also enhances the H_C values as shown in figure 5(b). Compared with the continuous thin films deposited on MgO and with other different substrates, the H_C values are significantly higher for nanohole arrays [21, 24].

Another noticeable behavior observed in the nanohole arrays is the ferromagnetic insulating phase at lower temperature which is contrary to the basic transport mechanism of the Sr-doped lanthanum manganite. In this manganite the ferromagnetic phase is always accompanied with metallic state because of the double exchange (DE) pairs of Mn^{3+} and Mn^{4+}. Such a DE mechanism was explained by Zener [30], where the conductivity is attributed to an electron hopping from Mn^{3+} to O^{2-} which is accompanied by a simultaneous hop from the later to Mn^{4+}. Since the exchange is carried out through Mn–O–Mn chain, the Mn–O bond length and Mn–O–Mn bond angle are considered as important parameters in manganites. However, the DE is only possible when t_{2g} spins are aligned in a parallel manner that explains the coexistence of ferromagnetism and metallic phases. According to Anderson and Hasegwa [31], the hopping amplitude (t) of the e_g electron from one site to another is a function of relative spin alignment at the two sites that can be expressed as $t = t_0\cos(\theta/2)$, where θ is the angle between the neighboring t_{2g} spins. Thus, the hopping amplitude is maximum when the spins are aligned parallel ($\theta = 0$), and zero for antiparallel alignment ($\theta = 180°$).

As mentioned earlier, the presence of voids leads to a spin misalignment state in the vicinity of nanoholes which could be a result from the significant changes in the Mn–O bond length and Mn–O–Mn bond angle. Such changes will modify the spin ordering in the MnO_2 plane which is an important channel for charge transport [32]. According to these changes, the MnO_6 octahedra can be tilted and this leads to a canted spin state. In our case, the tilted MnO_6 octahedra do not participate effectively in DE due to their canted spin configuration ($\theta \neq 0$). Thus, we have observed a canted ferromagnetic insulating (CFI) phase induced by the voids which restricts and suppresses the ferromagnetic DE interaction. Such a canted ferromagnetic state in perovskite manganites has already been studied theoretically and

experimentally by several researchers [33, 34]. Previous reports suggest that such a canted ferromagnetic state may evolve from an antiferromagnetic state [35]. However, our experimental results reported here do not support the existence of antiferromagnetic order which can be evidenced from the $M(T)$ and $M(H)$ curves measured for LSMO nanohole arrays. In consequence, the LSMO nanohole arrays exhibit a canted ferromagnetic insulating phase at low temperatures and a paramagnetic insulating state above T_C.

The magnetic phase separation is a prominent behavior of perovskite manganites which is characterized by multiple phases of different magnetic properties that can coexist within a single and chemically pure phase. Such phase separation is an important phenomenon for the applications of manganites in functional devices which can be induced by internal pressure by changing the dopant and the doping concentration, as well by external pressure such as hydrostatic pressure [36, 37]. However, the phase separation in LSMO nanohole arrays is obtained by introducing the artificial defects and such spin states engineering can be used to improve the functional properties of perovskite materials.

4. Conclusion

In summary, we have shown that the multicomponent oxide nanohole arrays can be synthesized by template assisted pulsed laser ablation method by performing the fabrication of LSMO nanohole arrays. The structural studies by SEM, AFM, EDS and XRD show well ordered and periodic arrays of nanoholes with single phase $La_{0.7}Sr_{0.3}MnO_3$. The magnetic and electrical resistance measurements hinted a canted ferromagnetic insulating phase at lower temperature and suggest a magnetic phase separation between ferromagnetic and canted ferromagnetic states. In addition, the presence of voids was found to be reducing the ferromagnetic exchange interaction resulting in an insulating phase. Moreover, the increased H_C compared to continuous LSMO/MgO film indicates an enhancement of magnetic pinning effect in the vicinity of nanoholes. As a consequence, the reported fabrication process obviates the need for high cost lithography and sputtering to produce such multicomponent oxide nanohole arrays and open new pathways for the growth of more multicomponent oxide nanostructures on NPA template to investigate their suitability for spin-based devices.

Acknowledgments

M K is thankful to FCT, Portugal for the Grant No. SFRH/BPD/75110/2010. The authors acknowledged the financial supports from the projects NORTE-07–0124-FEDER-000070, CERN/FIS-NUC/0004/2015 and IF/00686/2014.

References

[1] Yoon-Bong H, Ahmad R and Tripathy N 2012 Chemical and biological sensors based on metal oxide nanostructures *Chem. Commun.* **48** 10369

[2] Sousa C T, Nunes C, Proenca M P, Leitao D C, Lima J L F C, Reis S, Araujo J P and Lucio M 2012 pH sensitive silica nanotubes as rationally designed vehicles for NSAIDs delivery *Colloids Surf.* B **94** 288

[3] Wang D, Ding N, Song X H and Chen C H 2009 A simple gel route to synthesize nano-$Li_4Ti_5O_{12}$ as a high-performance anode material for Li-ion batteries *J. Mater. Sci.* **44** 198

[4] Rosei F 2004 Nanostructured surfaces: challenges and frontiers in nanotechnology *J. Phys.: Condens. Matter* **16** S1373

[5] Rahman M T, Dumas R K, Eibagi N, Shams N N, Yun-Chung W, Liu K and Chih-Huang L 2009 Controlling magnetization reversal in Co/Pt nanostructures with perpendicular anisotropy *Appl. Phys. Lett.* **94** 042507

[6] Leitao D C, Ventura J, Teixeira J M, Sousa C T, Pinto S, Sousa J B, Michalik J M, De Teresa J M, Vazquez M and Araujo J P 2013 Correlations among magnetic, electrical and magneto-transport properties of NiFe nanohole arrays *J. Phys.: Condens. Matter* **25** 066007

[7] Merazzo K J, Leitao D C, Jimenez E, Araujo J P, Camarero J, del Real R P, Asenjo A and Vazquez M 2011 Geometry-dependent magnetization reversal mechanism in ordered Py antidot arrays *J. Phys. D: Appl. Phys.* **44** 505001

[8] Jalil M B A 2003 Bit isolation in periodic antidot arrays using transverse applied fields *J. Appl. Phys.* **93** 7053

[9] Cowburn R P, Adeyeye A O and Bland J A C 1997 Magnetic domain formation in lithographically defined antidot Permalloy arrays *Appl. Phys. Lett.* **70** 2309

[10] Klein M J K, Guillaumee M, Wenger B, Dunbar L A, Brugger J, Heinzelmann H and Pugin R 2010 Inexpensive and fast wafer-scale fabrication of nanohole arrays in thin gold films for plasmonics *Nanotechnology* **21** 205301

[11] Leitao D C, Ventura J, Sousa C T, Teixeira J M, Sousa J B, Jaafar M, Asenjo A, Vazquez M, De Teresa J M and Araujo J P 2012 Tailoring the physical properties of thin nanohole arrays grown on flat anodic aluminum oxide templates *Nanotechnology* **23** 425701

[12] Kovylina M, Erekhinsky M, Morales R, Villegas J E, Schuller I K, Labarta A and Batlle X 2009 Tuning exchange bias in Ni/FeF_2 heterostructures using antidot arrays *Appl. Phys. Lett.* **95** 152507

[13] Konstantinovic Z, Santiso J, Colson D, Forget A, Balcells L and Martìnez B 2009 Self-organization processes in highly epitaxial $La_{2/3}Sr_{1/3}MnO_3$ thin films grown on $SrTiO_3$(001) substrates *J. Appl. Phys.* **105** 063919

[14] Sousa C T, Leitao D C, Proenca M P, Ventura J, Pereira A M and Araujo J P 2014 Nanoporous alumina as templates for multifunctional applications *Appl. Phys. Rev.* **1** 031102

[15] Sun J Z, Gallagher W J, Duncombe P R, Krusin-Elbaum L, Altman R A, Gupta A, Lu Y, Gong G Q and Xiao G 1996 Observation of large low field magnetoresistance in trilayer perpendicular transport devices made using doped manganate perovskites *Appl. Phys. Lett.* **69** 3266

[16] Volkov N V 2012 Spintronics: manganite-based magnetic tunnel structures *Phys. Usp.* **55** 250

[17] Jiang S P 2008 Development of lanthanum strontium manganite perovskite cathode materials of solid oxide fuel cells: a review *J. Mater. Sci.* **43** 6799

[18] Kale S N, Rajagopal R, Arora S, Bhayani K R, Rajwade J M, Paknikar K M, Kundaliya D C and Ogale S B 2007 Microwave Response of $La_{0.7}Sr_{0.3}MnO_3$ Nanoparticles for Heating Applications *J. Biomed. Nanotechnol.* **3** 178

[19] Kumaresavanji M, Sousa C T, Pires A, Pereira A M, Lopes A M L and Araujo J P 2014 Room temperature magnetocaloric effect and refrigerant capacitance in $La_{0.7}Sr_{0.3}MnO_3$ nanotube arrays *Appl. Phys. Lett.* **105** 083110

[20] Proenca M P, Sousa C T, Leitao D C, Ventura J, Sousa J B and Araujo J P 2008 Nanopore formation and growth in phosphoric acid Al anodization *J. Non-Cryst. Solids.* **354** 5238

[21] Mota D A *et al* 2014 Unravelling the effect of $SrTiO_3$ antiferrodistortive phase transition on the magnetic properties of $La_{0.7}Sr_{0.3}MnO_3$ thin films *J. Phys. D: Appl. Phys.* **47** 435002

[22] Gomes I T, Almeida B G, Lopes A M L, Araujo J P, Barbosa J and Mendes J A 2010 Structural and magnetic characterization of $LaSrMnO_3$ thin films deposited by laser ablation on MgO substrates *J. Mag. Mag. Mat.* **322** 1174

[23] Conceicao L d and Souza M M V M 2013 Synthesis of $La_{0.7}Sr_{0.3}MnO_3$ thin films supported on Fe-Cr alloy by sol-gel/dip-coating process: Evaluation of deposition parameters *Thin Solid Films* **534** 218

[24] Majumdar S, Huhtinen H, Majumdar H S and Paturi P 2012 Stress and defect induced enhanced low field magnetoresistance and dielectric constant in $La_{0.7}Sr_{0.3}MnO_3$ thin films *J. Alloys Compd.* **512** 332

[25] Gupta A, Gong G Q, Gang Xiao P R, Duncombe P, Lecoeur P, Trouilloud Y Y, Wang V P, Dravid and Sun J Z 1996 Grain-boundary effects on the magnetoresistance properties of perovskite manganite films *Phys. Rev.* B **54** R15629

[26] Liu S M, Zhu X B, Yang J, Song W H, Dai J M and Sun Y P 2006 The effect of grain boundary on the properties of $La_{0.7}Sr_{0.3}MnO_3$ thin films prepared by chemical solution deposition *Ceram. Int.* **32** 157

[27] Sheng P, Abeles B and Arie Y 1973 Hopping conductivity in granular metals *Phys. Rev. Lett.* **31** 44

[28] Julliere M 1975 Tunneling between ferromagnetic films *Phys. Lett.* A **54** 225

[29] Navas D, Ilievski F and Ross C A 2009 CoCrPt aintidot arrays with perpendicular magnetic anisotropy made on anodic alumina templates *J. Appl. Phys.* **105** 113921

[30] Zener C 1951 Interaction between the d-Shells in the transition metals: II. Ferromagnetic compounds of manganese with perovskite structure *Phys. Rev.* **82** 403

[31] Anderson P W, Hill M and Hasegawa H 1955 Considerations on Double Exchange *Phys. Rev.* **100** 675

[32] Alonso J A, Martinez-Lope M J, Casais M T and Fernandez-Diaz M T 2000 Evolution of the Jahn Teller Distortion of MnO_6 Octahedra in $RMnO_3$ Perovskites (R = Pr, Nd, Dy, Tb, Ho, Er, Y): A Neutron Diffraction Study *Inorg. Chem.* **39** 917

[33] Khutsishvili K O and Fokina N P 2010 Colossal magnetoresistance mechanism in doped manganites based on the canted ferromagnetic phase *J. Appl. Phys.* **107** 09B109

[34] Argyriou D N, Mitchell J F, Potter C D, Hinks D G, Jorgensen J D and Bader S D 1996 Lattice effects and magnetic order in the canted ferromagnetic insulator $La_{0.875}Sr_{0.125}MnO_{3+\delta}$ *Phys. Rev. Lett.* **76** 3826

[35] de Gennes P-G 1960 Effects of double exchange in magnetic crystals *Phys. Rev.* **118** 141

[36] Kumaresavanji M, Sousa L L L, Machado F L A, Adriano C, Pagliuso P G, Saitovitch E M B and Fontes M B 2010 Effects of Ru doping on the transport and magnetic properties of a $La_{1.32}Sr_{1.68}Mn_{2-y}Ru_yO_7$ layered manganite system *J. Phys.: Condens. Matter* **22** 236003

[37] Malavasi L, Baldini M, Zardo I, Hanfland M and Postorino P 2009 Pressure induced phase separation in optimally doped bilayer manganites *Appl. Phys. Lett.* **94** 061907